ACADEMIC PRESS

Available online at www.sciencedirect.com

SCIENCE DIRECT®

Journal of Sound and Vibration 263 (2003) 47–68

JOURNAL OF SOUND AND VIBRATION

www.elsevier.com/locate/jsvi

Sound wave motion in pipes having time-variant ambient temperature

E. Dokumaci*

Department of Mechanical Engineering, Dokuz Eylul University, Bornova, Izmir, Turkey

Received 18 October 2001; accepted 6 June 2002

Abstract

The classical time-invariant acoustic waveguide theory is extended by allowing for temporal variations of the speed of sound. Essentially, what distinguishes the present theory from the classical waveguide theory is that, while the latter predicts stable waves for all frequencies, the present theory predicts that stable waves may occur only in certain frequency bands. Implication of the theory for engine exhaust pipes is discussed.

1. Introduction

In the classical time-invariant theory of isentropic acoustic waveguides [1], the propagation is assumed to take place in a medium having a temporally constant speed of sound. The present paper aims to extend this theory by taking into account the possible temporal variations of the speed of sound. The problem adopted for this purpose is the sound wave propagation in a uniform straight duct of arbitrary cross-section, with rigid impervious walls and having a uniform mean temperature along its length, but this temperature varying periodically in time. The effect of visco-thermal losses is neglected and the mean flow is assumed to be uniform. As far as the author is aware, no one has published on this problem, hitherto.

Essentially, what distinguishes the present theory from the classical waveguide theory is that while the latter predicts stable waves for all frequencies, the present theory predicts that stable waves may occur only in certain frequency bands. The analysis, while showing the nature of stable sound wave motion, focuses on determination of the conditions that give rise to unstable wave motion. Stability charts are presented for periodic rectangular and right-triangular pulse models of ambient temperature variations.

*Tel.: +232-388-7868; fax: +232-388-7864.
E-mail address: dokumaci@deu.edu.tr (E. Dokumaci).

0022-460X/03/$ - see front matter
doi:10.1016/S0022-460X(02)01097-0

The present theory has some relevance to engine exhaust noise as the temperature condition envisaged in the theory is satisfied approximately in exhaust pipes. The paper includes a discussion on the implications of the theory for engine exhaust pipes.

2. Time-variant wave equation

Upon assuming a perfect gas and neglecting visco-thermal effects, isentropic wave motion in a pipe is governed by the classical fluid dynamic conservation equations for mass and momentum, which, upon using the state equation $\mathrm{d}p = c^2\,\mathrm{d}\rho$ with $c^2 = \gamma p/\rho$, can be expressed as

$$\frac{\partial p}{\partial t} + \mathbf{v}\cdot\nabla p + \gamma p\nabla\cdot\mathbf{v} = 0, \tag{1}$$

$$\gamma p\left(\frac{\partial \mathbf{v}}{\partial t} + \mathbf{v}\cdot\nabla\mathbf{v}\right) + c^2\nabla p = 0, \tag{2}$$

where p is the pressure, ρ is fluid density, $\mathbf{v}$ is particle velocity, t denotes time, c^2 is the speed of sound squared and γ is the ratio specific heat coefficients. The equations that govern the propagation of sound waves in a pipe having time-varying ambient temperatures come from the linearization of Eqs. (1) and (2) by

$$p(t,\mathbf{x}) = p_o + p'(t,\mathbf{x}), \qquad \mathbf{v}(t,\mathbf{x}) = \mathbf{v}_o + \mathbf{v}'(t,\mathbf{x}), \qquad c^2(t,\mathbf{x}) = c_o^2(t). \tag{3}$$

Here, $\mathbf{x}$ denotes Cartesian position co-ordinates (x_1, x_2, x_3), and p' and $\mathbf{v}'$ denote, respectively, the fluid pressure and particle velocity due to acoustic wave motion, which are assumed to be small perturbations of the first order. The temperature fluctuations associated with the wave motion are assumed to have negligible effect on the speed of sound squared. The ambient pressure, p_o, the mean flow velocity, $\mathbf{v}_o$, and γ are assumed to be constant and spatial ambient temperature gradients are neglected. Then, the speed of sound squared may be assumed to be a function of only time, periodic with period T, which is tantamount to assuming that the ambient temperature is a periodic function of time of the same period. Upon substituting Eqs. (3), Eqs. (1) and (2) can be expressed to first order as

$$\frac{\partial p'}{\partial t} + \mathbf{v}_o\cdot\nabla p' + \gamma p_o\nabla\cdot\mathbf{v}' = 0, \tag{4}$$

$$\gamma p_o\left(\frac{\partial \mathbf{v}'}{\partial t} + \mathbf{v}_o\cdot\nabla\mathbf{v}'\right) + c_o^2\nabla p' = 0, \tag{5}$$

respectively. Elimination of the particle velocity then gives

$$\left[\nabla^2 - \frac{1}{c_o^2}\left(\frac{\partial}{\partial t} + \mathbf{v}_o\cdot\nabla\right)^2\right]p' = 0. \tag{6}$$

This convected wave equation, which is well known for the constant speed of sound case [1,2], is not separable for the time dependency; however, under the Galilean transformation

$$\mathbf{y} = \mathbf{x} - \mathbf{v}_o t, \qquad \tau = t, \tag{7}$$

it reduces to the wave equation

$$\left(\nabla_{\mathbf{y}}^2 - \frac{1}{c_o^2}\frac{\partial^2}{\partial\tau^2}\right)p' = 0, \qquad \nabla_{\mathbf{y}} = \left(\frac{\partial}{\partial y_1}, \frac{\partial}{\partial y_2}, \frac{\partial}{\partial y_3}\right), \tag{8}$$

which is separable as

$$p'(\mathbf{y}, \tau) = P(\mathbf{y})q(\tau). \tag{9}$$

Here, the separating functions are given by

$$(\nabla_y^2 + K^2)P(\mathbf{y}) = 0, \tag{10}$$

$$\left[\frac{\mathrm{d}^2}{\mathrm{d}\tau^2} + K^2 c_o^2(\tau)\right]q(\tau) = 0, \tag{11}$$

where K^2 denotes a constant. The present study is restricted to real and positive values of this constant.

Eq. (10) is the classical Helmholtz equation. Assuming axial mean flow, $\mathbf{v}_o = (v_{o1}, 0, 0)$, x_1 being the pipe axis, its solution can be expressed, again by the method of separation of variables, in the single-mode form

$$P(\mathbf{y}) = B^{\mp}\Psi(y_2, y_3)\exp\left(\mp \mathrm{i}\sqrt{K^2 - \alpha^2}y_1\right) = P^{\mp}(\mathbf{y}). \tag{12}$$

Here, $B^{\pm}$ denote integration constants and the solutions associated with the upper and lower signs of the square root are indicated by using the corresponding upper and lower signs as superscripts. This convention is used throughout the paper. In Eq. (12), i denotes the unit imaginary number, and α and Ψ denote, respectively, the eigenvalues and the corresponding eigenfunctions, for given pipe wall boundary condition, of the two-dimensional Helmholtz equation:

$$\left(\frac{\partial^2}{\partial y_2^2} + \frac{\partial^2}{\partial y_3^2} + \alpha^2\right)\Psi = 0. \tag{13}$$

Exact and approximate solutions of this equation are available for a large number of geometries. For example, for circular hard-walled ducts of radius r, separable solution of the foregoing equation can be expressed as

$$\Psi(y_2, y_3) = \mathrm{J}_m(\alpha_{mn}y_2)\begin{cases}\cos my_3, \\ \sin my_3,\end{cases} \qquad m = 0, 1, 2, \ldots, \quad n = 1, 2, \ldots, \tag{14}$$

where J_m denotes a Bessel function of order m and the smallest values of α_{mn} are: $r\alpha_{01} = 0$, $r\alpha_{11} = 1.841$, $r\alpha_{21} = 3.054$, $r\alpha_{02} = 3.832$, … . This solution holds in polar co-ordinates; i.e., y_2 and y_3 represent, respectively, the radial and angular co-ordinates.

Eq. (11), on the other hand, is the classical Hill equation, solution of which is, by Floquet theory [3], of the form,

$$q(\tau) = \varphi(\tau)\exp\lambda\tau, \qquad \lambda = \frac{\ln\sigma}{T}. \tag{15}$$

Here, σ denotes an eigenvalue of the monodromy matrix, $\mathbf{U}(T)$, of Eq. (11), which is defined by $\mathbf{q}(\tau + T) = \mathbf{U}(T)\mathbf{q}(\tau)$, where $\mathbf{q}(\tau) = \{q(\tau)\,\mathrm{d}q/\mathrm{d}\tau\}$. If the two eigenvalues of $\mathbf{U}(T)$ have linearly independent eigenvectors, then $\varphi(\tau)$ is a periodic bounded function of period T; else, $\varphi(\tau)$ is a

linear polynomial in τ with periodic bounded coefficients of period T. The latter case occurs if the two eigenvalues of $\mathbf{U}(T)$ are equal and the corresponding eigenvectors are linearly dependent.

Upon combining Eqs. (12) and (15), the single-mode solution of Eq. (8) can be expressed as a sum of the complex pressure wave components

$$p^{\mp}(\mathbf{y},\tau) = B^{\mp}\Psi(y_2,y_3)\exp\left(\mp \mathrm{i}\sqrt{K^2-\alpha^2}y_1\right)\varphi(\tau)\exp\lambda\tau, \tag{16}$$

where the real part of the complex solution is understood to be relevant as usual.

To complete this solution, it remains to derive the corresponding expression for the particle velocity. For this purpose, it is convenient to introduce the velocity potential $\phi'(\mathbf{x},t)$, which is defined by $\mathbf{v}' = \nabla\phi'$. The following wave equation for the velocity potential can be derived by recasting Eqs. (4) and (5) in terms of ϕ' and then eliminating p':

$$\left[\nabla^2 - \left(\frac{\partial}{\partial t} + \mathbf{v}_o\cdot\nabla\right)\frac{1}{c_o^2}\left(\frac{\partial}{\partial t} + \mathbf{v}_o\cdot\nabla\right)\right]\phi' = 0, \tag{17}$$

or, in the moving co-ordinate frame defined by transformation (7),

$$\left(\nabla_{\mathbf{y}}^2 - \frac{\partial}{\partial\tau}\frac{1}{c_o^2}\frac{\partial}{\partial\tau}\right)\phi' = 0. \tag{18}$$

As can be proved by substitution, the separable solution of this wave equation that also satisfies Eqs. (4) and (5) is

$$\phi'(\mathbf{y},\tau) = \frac{1}{K^2 p_o\gamma}P(\mathbf{y})\frac{\mathrm{d}}{\mathrm{d}\tau}q(\tau). \tag{19}$$

Here, $P(\mathbf{y}), q(\tau)$ and K are as defined by Eqs. (10) and (11). Thus, the components of the particle velocity, $\mathbf{v}' = (v_1', v_2', v_3')$, are given by

$$v_j'(\mathbf{y},\tau) = \frac{1}{K^2 p_o\gamma}\left[\frac{\partial}{\partial y_j}P(\mathbf{y})\right]\frac{\mathrm{d}}{\mathrm{d}\tau}q(\tau), \quad j = 1,2,3. \tag{20}$$

In particular, the axial component of the particle velocity, v_1', can be expressed as the sum of the velocity components

$$v_1^{\mp}(\mathbf{y},\tau) = \frac{\mp \mathrm{i}\sqrt{K^2-\alpha^2}}{K^2 p_o\gamma}\left[\lambda + \frac{\mathrm{d}\varphi}{\varphi\mathrm{d}\tau}\right]p^{\mp}(\mathbf{y},\tau). \tag{21}$$

The solution of the wave equation (6) can now be obtained by transforming Eqs. (16) and (20) back to the fixed frame. However, it is convenient to consider first the question of the stability of the wave motion.

3. Stability of the wave motion

The perturbation formulation adopted in the present study is tantamount to viewing the fluid particles as undergoing a wave motion while being convected along the duct with a uniform velocity. Therefore, the stability, or instability, of the wave motion is decided by whether the wave amplitudes remain bounded in time, or increase without bound, for an observer moving with the

mean flow. Hence, the characteristic exponent λ, which is defined by the second of Eqs. (15), is the determining parameter in the present stability considerations.

An important property of Eq. (11) is that its monodromy matrix, $\mathbf{U}(T)$, is reciprocal. This means that, if an eigenvalue of $\mathbf{U}(T)$ is σ, then $1/\sigma$ is also an eigenvalue; that is, the characteristic equation of $\mathbf{U}(T)$ will be of the form

$$\sigma^2 + a_1\sigma + 1 = 0, \tag{22}$$

where a_1 denotes a physical parameter. A proof of this can be found in the book by Bolotin [3]. Then, the eigenvalues of $\mathbf{U}(T)$, σ_1 and σ_2, say, must satisfy $\sigma_1\sigma_2 = 1$. Therefore, if one of the eigenvalues of $\mathbf{U}(T)$ is real and different from unity in absolute value, the wave motion will be unstable. If, on the other hand, one of the eigenvalue of $\mathbf{U}(T)$ is complex, then the other must be its complex conjugate and, moreover, both eigenvalues must be of modulus unity. Therefore, if an eigenvalue of $\mathbf{U}(T)$ is complex, the wave motion will be stable. The only remaining possibility is that one of the eigenvalues of $\mathbf{U}(T)$ is real and equal to unity in absolute value. In this case, the wave motion may be stable, or unstable, depending on whether the corresponding eigenvectors are linearly independent, or linearly dependent. It can be shown that the criteria for stable and unstable solutions are bounded by the conditions $\sigma_1 = \sigma_2 = +1$ and $\sigma_1 = \sigma_2 = -1$, which correspond, respectively, to periodic solutions of period T and $2T$ of the Hill equation [3].

The prevalence of the foregoing conditions and the characteristics of the stable wave motion are studied further in the next section. Strictly speaking, the study of the time evolution and propagation of unstable waves are beyond the scope of the present analysis. Eq. (16) shows that, initially, the unstable modes will be in the form of exponentially growing waves, the rate of growth in time being equal to the characteristic exponent (in the case of instability with equal characteristic exponents, growth with time is linear). As amplitudes increase, however, non-linear effects will intervene and determine the time evolution and the form of propagation of the wave motion, the prediction of which requires the solution of the parent non-linear conservation equations, Eqs. (1) and (2).

3.1. Approximate harmonic balance analysis

Preliminary observations on the conditions under which unstable propagating waves may prevail can be made by applying the fact that the stability boundaries are given by the periodic solutions of Eq. (11) of periods T and $2T$. These periodic solutions can be sought in the form

$$q(t) = \sum_{m=0}^{\infty} \left(a_m \cos\frac{m\Omega t}{2} + b_m \sin\frac{m\Omega t}{2} \right), \quad \Omega = \frac{2\pi}{T}, \tag{23}$$

where a_m and b_m are the Fourier coefficients and one takes the sub-series for $m = 1, 3, 5, \ldots$ as the solution with period T and the sub-series for $m = 0, 2, 4, 6, \ldots$ as the solution with period $2T$. Periodic variations of the speed of sound can be expressed also in the form of a Fourier series:

$$c_o^2(t) = \bar{c}_o^2 \left(1 + \beta^2 \sum_{n=1}^{\infty} \mu_n \cos n\Omega t \right). \tag{24}$$

Here, for simplicity, a half-range expansion with Fourier coefficients μ_n is assumed; overbar denotes a mean value and $\beta^2 = C_o^2/\bar{c}_o^2$, where $2C_o^2$ is the peak-to-peak amplitude of the temporal

variations of the speed of sound squared, which is directly proportional to the peak-to-peak amplitude of the corresponding ambient temperature variations, the constant of proportionality being equal to γR, where R denotes the gas constant. The equations defining the boundaries of stability can be derived by the method of harmonic balance, which consists of substituting Eqs. (23) and (24) into Eq. (11) and balancing the coefficients of the harmonic terms having the same order. This results in a homogeneous system of an infinite number of linear equations for the coefficients a_m and b_m, and the condition for the existence of a non-trivial solution of which gives the equations of the boundaries of stability. In general, a closed form solution cannot be derived in this way due to the coupling between the harmonic terms in Eq. (24). If, however, this coupling is neglected, the equations of the stability boundaries can be expressed simply as

$$\eta = \frac{n}{\sqrt{1 \pm \frac{1}{2}\mu_n \beta^2}}, \qquad \eta = \frac{K\bar{c}_o}{\Omega/2}, \quad n = 1, 2, 3, \ldots, \tag{25}$$

which is adopted from Bolotin [3] with appropriate notational changes. The parameter η is called, for ease of reference, the stability number. Eq. (25) predicts that the regions of instability occur as in the stability chart sketched in Fig. 1(a), with vertices at $\eta = 1, 2, 3, \ldots$ on $\beta^2 = 0$ axis.

In this context, also relevant is the effect of damping on the regions of instability. For a qualitative conclusion, one may assume that the temporal effect of the presence of visco-thermal losses can be modelled by adding a small viscous damping term to the Hill equation. Then, the harmonic balance method predicts that the boundaries of stability given by Eq. (25) may be modified as depicted in Fig. 1(b). The presence of damping causes contraction of the regions of instability of the (undamped) Hill equation and the minimum β^2 required for instabilities to prevail become greater than zero. For example, if damping is added to Eq. (11) by the term $2\varepsilon\, \mathrm{d}q/\mathrm{d}t$, a similar approximate application of the harmonic balance method leading to Eq. (25) shows that the vertex of the instability region of order n occurs at $\beta^2_{min} = 8\varepsilon/\eta\Omega\mu_n$; that is,

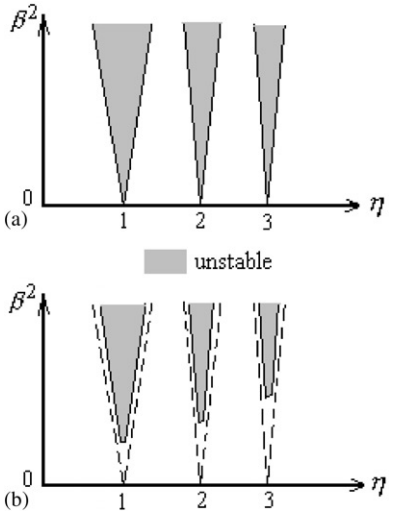

Fig. 1. Regions of instability.

β^2_{min}depends on μ_n and the relationship between ε and the stability number, and it need not necessarily increase with the order of the instability region, as implied in Fig. 1(b). Since damping, however small, is unavoidable in real systems, the boundaries of stability of Eq. (11) may be understood as close envelopes of actual boundaries.

3.2. Periodic rectangular pulse model of temperature variation

The simplicity of Eq. (25) is attractive but, there is no metric for how large β^2 can be taken without violating the underlying assumption that the effect of coupling between the harmonics of Eq. (24) is negligible. Effect of β^2 need to be known with less ambiguity for the assessment of the possible occurrence of wave instabilities. Several numerical methods are available, in addition to the method of harmonic balance, for accurate determination of the exact stability boundaries. The approach that is adopted in this study is a basic one and essentially consists of the integration of Eq. (11) over period T for the determination of its monodromy matrix, $\mathbf{U}(T)$. For this purpose, the temporal variation of the ambient temperature need to be known. In the present analysis, the temperature variations are modelled as periodic rectangular and triangular functions. For these functions, the monodromy matrix of Eq. (11) can be derived analytically.

The periodic rectangular function, shown in Fig. 2, presumes that the pipe temperature suddenly increases to a maximum, remains at that value for a fraction a of period T, and then suddenly drops down to its initial value. For this function, Eq. (11) is written as

$$\frac{\mathrm{d}^2q}{\mathrm{d}t^2} + \omega_1^2 q = 0, \qquad \omega_1^2 = K^2\bar{c}_o^2(1 + 2b\beta^2), \quad 0 < t \leqslant aT, \tag{26}$$

$$\frac{\mathrm{d}^2q}{\mathrm{d}t^2} + \omega_2^2 q = 0, \qquad \omega_2^2 = K^2\bar{c}_o^2(1 - 2a\beta^2), \quad aT < t \leqslant T, \tag{27}$$

where $a + b = 1$ and $2a\beta^2 < 1$. Solutions of these equations can be expressed as

$$q(t) = q(0)\cos\omega_1 t + \frac{\dot{q}(0)}{\omega_1}\sin\omega_1 t, \quad 0 < t \leqslant aT, \tag{28}$$

$$q(t_1) = q(aT)\cos\omega_2 t_1 + \frac{\dot{q}(aT)}{\omega_2}\sin\omega_2 t_1, \quad 0 < t_1 \leqslant bT, \tag{29}$$

respectively. Here, $t_1 = t - aT$ and an overdot denotes differentiation with respect to time. Hence, $q(T)$ and $\dot{q}(T)$ can be computed from Eqs. (28) and (29) in terms of the initial conditions at $t = 0$.

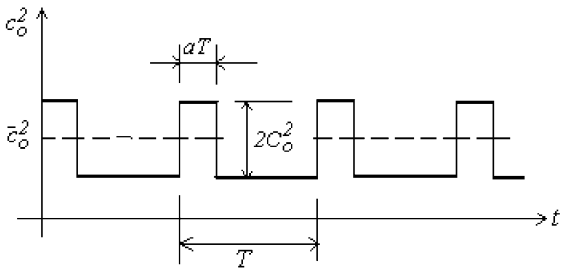

Fig. 2. Periodic rectangular pulse model of temporal temperature variations.

The result, expressed in matrix notation, is

$$\begin{bmatrix} q(T) \\ \dot{q}(T) \end{bmatrix} = \begin{bmatrix} U_{11} & U_{12} \\ U_{21} & U_{22} \end{bmatrix} \begin{bmatrix} q(0) \\ \dot{q}(0) \end{bmatrix}, \tag{30}$$

where the square matrix is the required monodromy matrix, $\mathbf{U}(T)$, the elements of which are

$$U_{11} = \cos\omega_1 aT \cos\omega_2 bT - \frac{\omega_1}{\omega_2} \sin\omega_1 aT \sin\omega_2 bT, \tag{31}$$

$$U_{12} = \frac{\sin\omega_1 aT \cos\omega_2 bT}{\omega_1} + \frac{\cos\omega_1 aT \sin\omega_2 bT}{\omega_2}, \tag{32}$$

$$U_{21} = -\omega_2 \cos\omega_1 aT \sin\omega_2 bT - \omega_1 \sin\omega_1 aT \cos\omega_2 bT, \tag{33}$$

$$U_{22} = -\frac{\omega_2}{\omega_1} \sin\omega_1 aT \sin\omega_2 bT + \cos\omega_1 aT \cos\omega_2 bT. \tag{34}$$

The eigenvalues of $\mathbf{U}(T)$ can be shown to be given by the roots of Eq. (22) with

$$a_1 = -2\cos\omega_1 aT \cos\omega_2 bT + \left(\frac{\omega_1}{\omega_2} + \frac{\omega_2}{\omega_1}\right) \sin\omega_1 aT \sin\omega_2 bT. \tag{35}$$

Thus, it follows that, if $|a_1| < 2$, the eigenvalues of $\mathbf{U}(T)$ are complex conjugate of modulus unity; if $|a_1| > 2$, they are real and not equal to unity in absolute value and, in view of the stability criteria given in the previous section, these conditions correspond to stable and unstable propagating waves, respectively. Hence, the boundaries separating the regions corresponding to stable and unstable propagating waves on the η versus β^2 plane are given by $|a_1| = 2$. Solution of this equation are presented in Figs. 3–5 as stability charts for $a = 0.1, 0.5$ and 0.8, respectively. Here, it may be noted that, for the rectangular function of Fig. 2, Fourier expansion gives $\mu_n = 4(\sin n\pi a)/n\pi$ and Eq. (25) does not provide a satisfactory representation of the boundaries of stability even when β^2 is relatively small, except for the region instability of order $n = 1$.

A stability chart based on a similar solution of the Hill equation has been given in Ref. [3] for $a = 0.5$. Fig. 4 agrees closely with that stability chart.

3.3. Periodic right triangular pulse model of temperature variation

The periodic triangular function, shown in Fig. 6, assumes that the pipe temperature suddenly increases to a maximum, then drops linearly to its initial value in a fraction a of period T. For this function, Eq. (11) is written as

$$\frac{d^2q}{dt^2} + (\omega_0^2 t + \omega_1^2)q = 0, \quad 0 < t \leqslant aT, \tag{36}$$

$$\frac{d^2q}{dt^2} + \omega_2^2 q = 0, \qquad \omega_2^2 = K^2\bar{c}_o^2(1 - a\beta^2), \quad aT < t \leqslant T, \tag{37}$$

where $a\beta^2 < 1$. In Eq. (36)

$$\omega_1^2 = K^2\bar{c}_o^2[1 + (2 - a)\beta^2], \qquad \omega_0^2 = -2K^2\bar{c}_o^2\beta^2/aT. \tag{38}$$

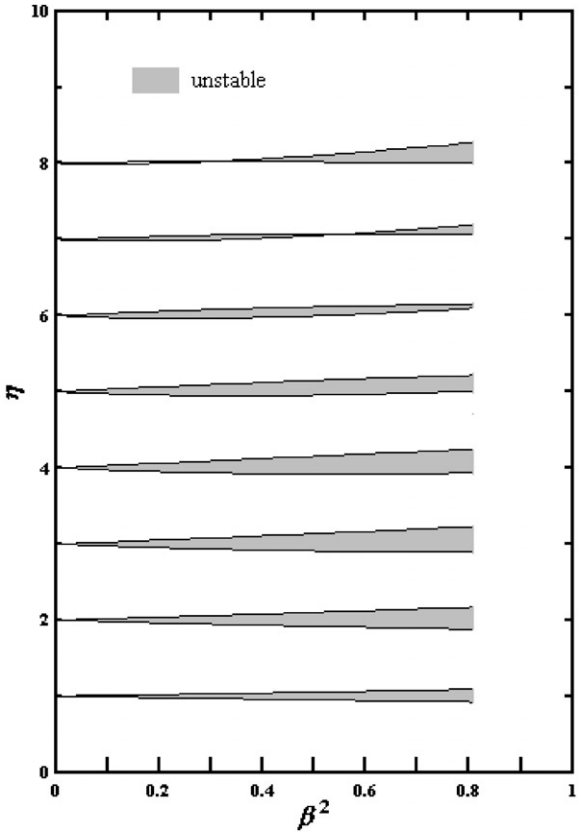

Fig. 3. Stability chart for a periodic rectangular temperature pulse with $a = 0.1$.

Solutions of Eqs. (36) and (37) can be expressed, respectively, as

$$q(t) = (2\omega_0/3)^{-1/3}\chi^{1/3}[A_1 \mathrm{J}_{1/3}(\chi(t)) + A_1 \mathrm{Y}_{1/3}(\chi(t))], \quad 0 < t \leqslant aT, \tag{39}$$

$$q(t_1) = q(aT)\cos\omega_2 t_1 + \frac{\dot{q}(aT)}{\omega_2}\sin\omega_2 t_1, \quad 0 < t_1 \leqslant bT. \tag{40}$$

In Eq. (39), which can readily be proved by back-substitution, A_1 and A_2 denote integration constants, J_v and Y_v denote, respectively, Bessel functions of order v of the first kind and second kind, and χ denotes the transformation

$$\chi(t) = (2\omega_0/3)(t + \omega_1^2/\omega_0^2)^{3/2}. \tag{41}$$

As can be shown by an analysis similar to that of Section 3.2, but with a preceding step of calculation of the integration constants A_1 and A_2 in Eq. (39) in terms of the initial conditions $q(0)$ and $\dot{q}(0)$, Eq. (30) holds with the monodromy matrix now given by

$$\mathbf{U}(T) = U_0 \begin{bmatrix} u_{11}\cos\omega_2 bT + u_{21}\dfrac{\sin\omega_2 bT}{\omega_2} & u_{12}\cos\omega_2 bT + u_{22}\dfrac{\sin\omega_2 bT}{\omega_2} \\ -u_{11}\omega_2\sin\omega_2 bT + u_{21}\cos\omega_2 bT & -u_{12}\omega_2\sin\omega_2 bT + u_{22}\cos\omega_2 bT \end{bmatrix}, \tag{42}$$

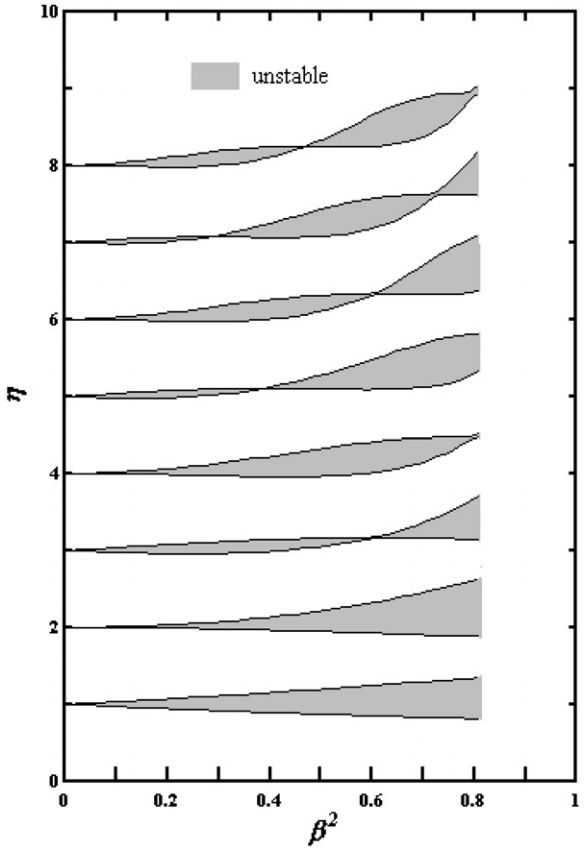

Fig. 4. Stability chart for a periodic rectangular temperature pulse with $a = 0.5$.

where

$$U_0 = \left[\frac{\chi(aT)}{\chi(0)}\right]^{1/3} \frac{1}{\mathrm{J}_{1/3}(\chi(0))\mathrm{Y}_{1/3}(\chi(0)) - \mathrm{J}_{-2/3}(\chi(0))\mathrm{Y}_{-2/3}(\chi(0))}, \tag{43}$$

$$u_{11} = \mathrm{J}_{1/3}(\chi(aT))\mathrm{Y}_{-2/3}(\chi(0)) - \mathrm{J}_{-2/3}(\chi(0))\mathrm{Y}_{1/3}(\chi(aT)), \tag{44}$$

$$u_{12} = [-\mathrm{J}_{1/3}(\chi(aT))\mathrm{Y}_{1/3}(\chi(0)) + \mathrm{J}_{1/3}(\chi(0))\mathrm{Y}_{1/3}(\chi(aT))]/[3\chi(0)\omega_0^2/2]^{1/3}(\Omega/2), \tag{45}$$

$$u_{21} = [\mathrm{J}_{-2/3}(\chi(aT))\mathrm{Y}_{-2/3}(\chi(0)) - \mathrm{J}_{-2/3}(\chi(0))\mathrm{Y}_{-2/3}(\chi(aT))] \times [3\chi(0)\omega_0^2/2]^{1/3}(\Omega/2), \tag{46}$$

$$u_{22} = -\mathrm{J}_{-2/3}(\chi(aT))\mathrm{Y}_{1/3}(\chi(0)) + \mathrm{J}_{1/3}(\chi(0))\mathrm{Y}_{-2/3}(\chi(aT)). \tag{47}$$

Therefore, in this case, the coefficient a_1 in Eq. (25) is

$$a_1 = (u_{11} + u_{22})\cos\omega_2 bT + \left(\frac{u_{21}}{\omega_2} - u_{12}\omega_2\right)\sin\omega_2 bT, \tag{48}$$

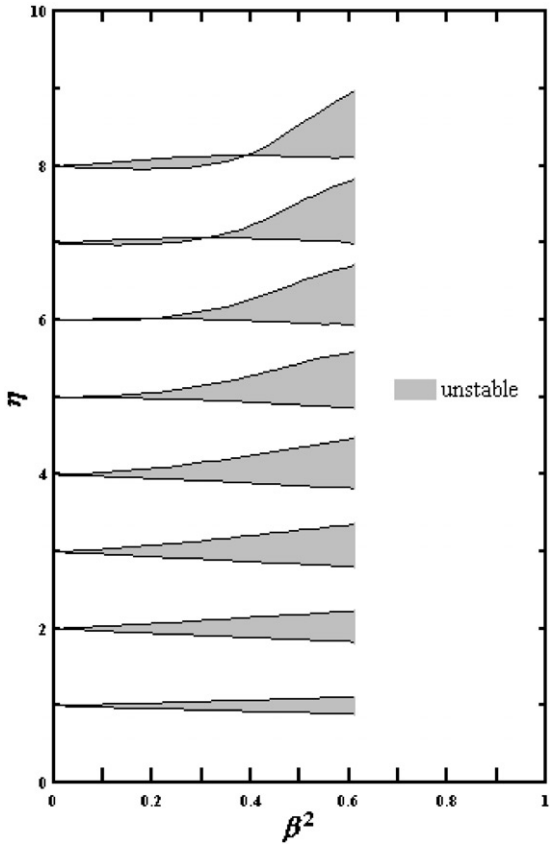

Fig. 5. Stability chart for a periodic rectangular temperature pulse with $a = 0.8$.

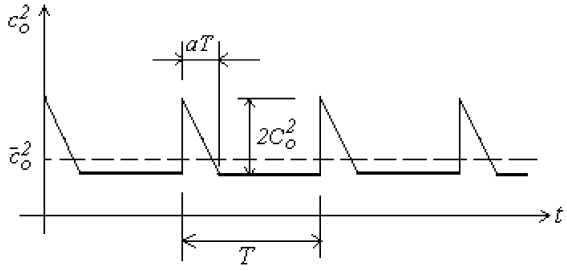

Fig. 6. Periodic right-triangular pulse model of temporal temperature variations.

which determines the boundaries of stability by $|a_1| = 2$. Solution of this equation is presented in Fig. 7 for $a = 0.5$ as a stability chart.

To the knowledge of the author, this solution of the Hill equation has not appeared elsewhere.

3.4. Time-domain characteristics of the wave motion

Analytical time-domain solutions of Eq. (11) have been given in the foregoing sections for periodic rectangular and right-triangular temperature variations. Although it is not the purpose of

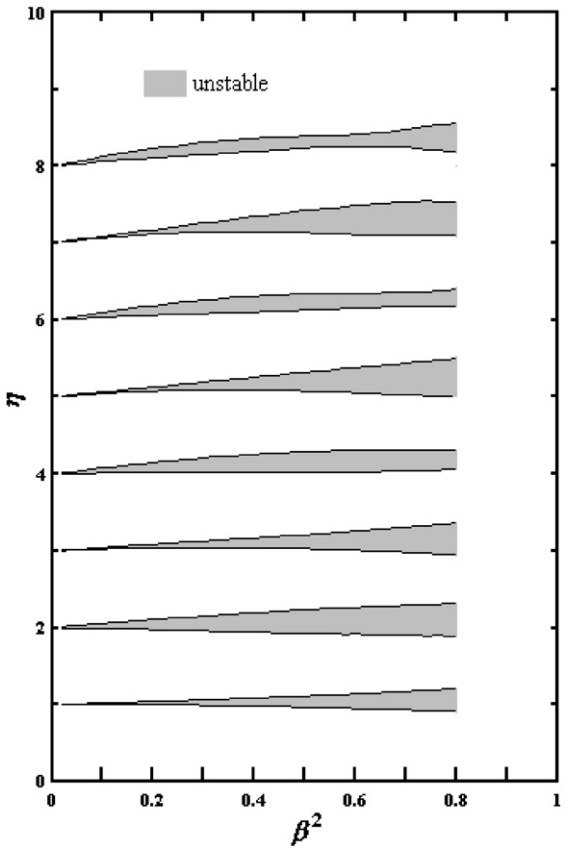

Fig. 7. Stability chart for a right-triangular temperature pulse with $a = 0.5$.

this paper to present an extensive examination of these solutions, it is important to note that some useful time-domain information can be inferred from the stability charts. To show this, it is sufficient to consider few cases of the solution for the periodic rectangular pulse model of the temperature variations.

As can be expected, as β^2 tends to zero, the present theory approaches the usual duct acoustics theory in which the speed of sound is assumed to be constant. Consequently, for relatively small values of β^2, the modulating function $\varphi(t)$ will tend to be a constant and the stable waves will be constant frequency waves, approximately. This can be observed in Fig. 8 which shows the time dependency of the stable waves for various values of β^2 on the $\eta = 2.5$ line of the stability chart for $a = 0.8$, Fig. 5. As β^2 increases, the $\eta = 2.5$ line comes closer to the boundaries of stability and the effect of modulation becomes more marked. This effect is shown further in Fig. 9, where the time dependency of the waves are shown for various values of the stability number, η, along the $\beta^2 = 0.4$ line of the same stability chart. The values of the stability number considered span across the region of instability of order $n = 3$ by points well into the next regions of stability and close to the two sides of the boundaries of stability, so that both the modulation effect and the passage to instability are observed. Finally, shown in Fig. 10, is the time evolution of the unstable waves in

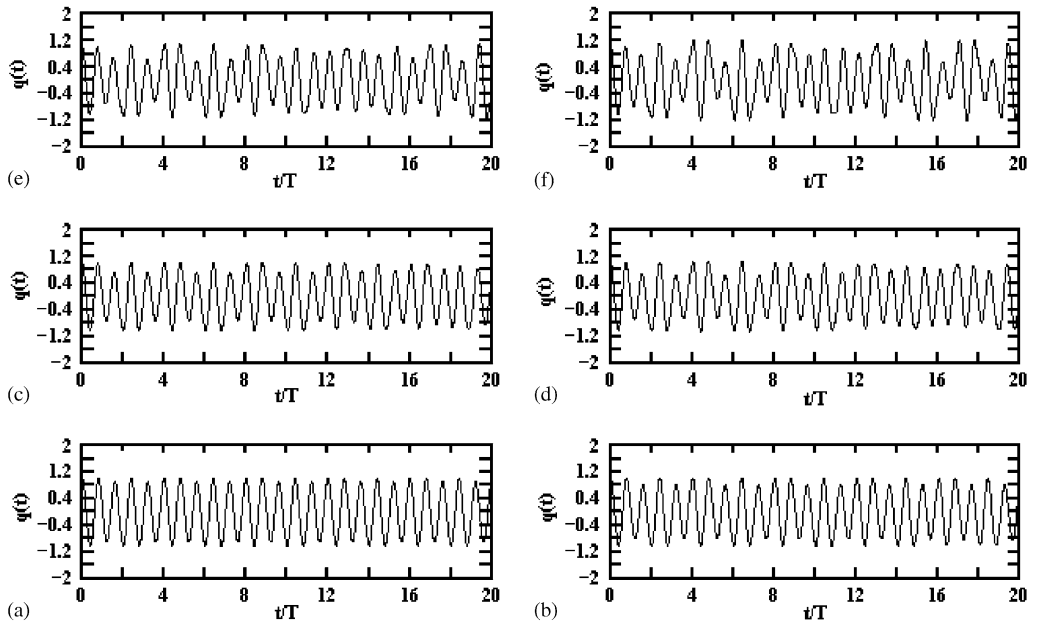

Fig. 8. Time dependency of stable propagating waves for periodic rectangular temperature variation. $a = 0.8$, $\eta = 2.5$ and $\beta^2 = 0.1$ (a), 0.2 (b), 0.3 (c), 0.4 (d), 0.5 (e), 0.6 (f).

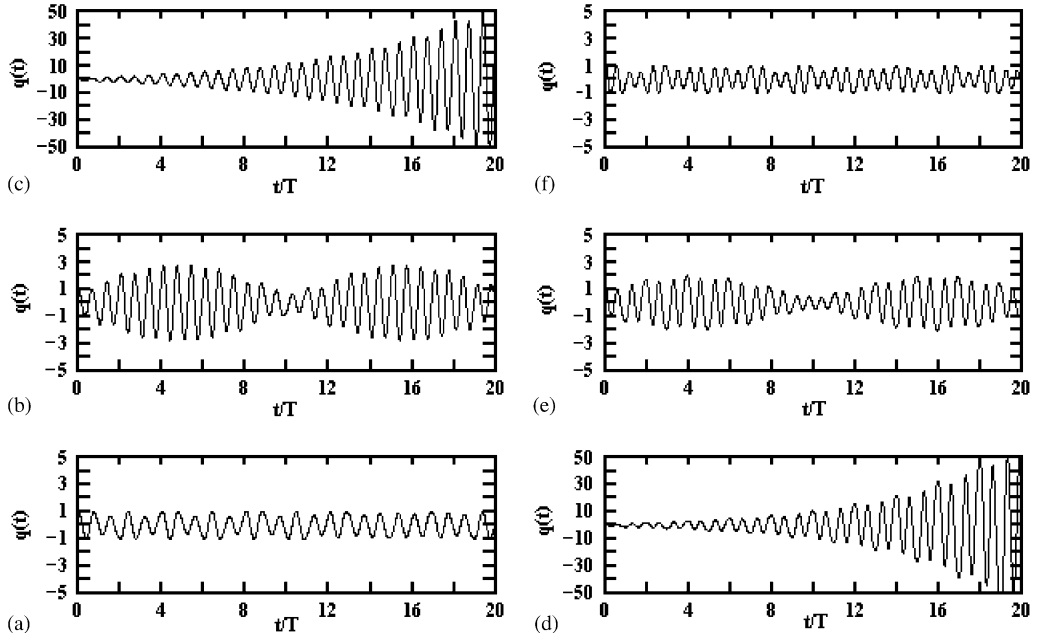

Fig. 9. Time dependency of wave motion for periodic rectangular temperature variation. $a = 0.8$, $\beta^2 = 0.4$ and $\eta = 2.5$ (a), 2.85 (b), 2.875 (c), 3.2 (d), 3.23 (e), 3.25 (f). See Fig. 10 for points very close to the boundaries of stability.

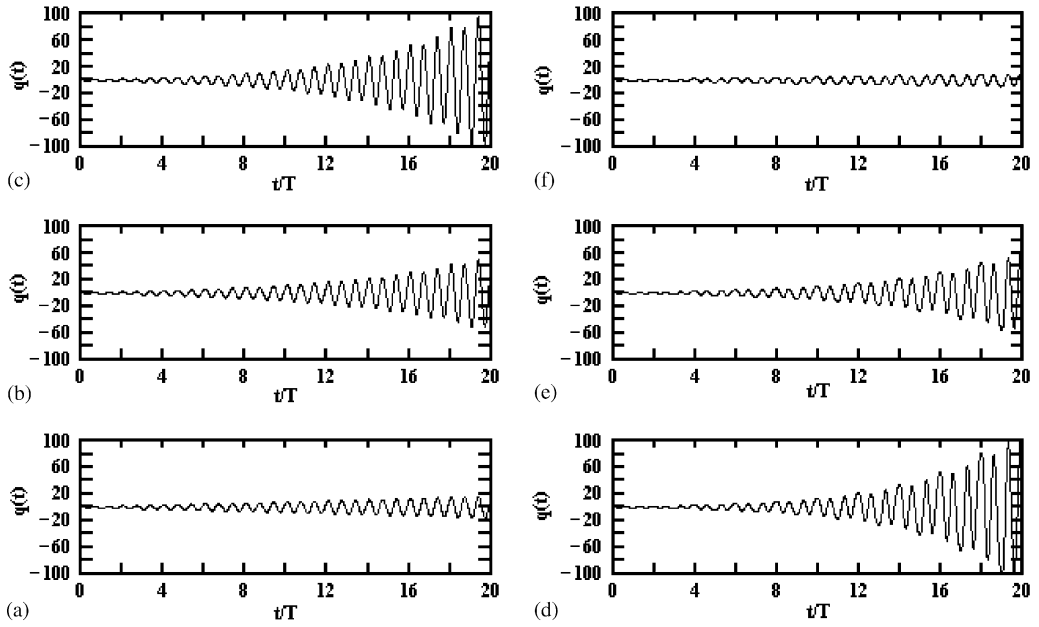

Fig. 10. Time dependency of wave motion for periodic rectangular temperature variation. $a = 0.8$, $\beta^2 = 0.4$ and $\eta =$ 2.8734 (a), 2.88 (b), 2.885 (c), 3.195 (d), 3.19 (e), 3.2102 (f). The first (a) and last (f) cases correspond to points very close to stability boundaries.

the same region of instability, along the $\beta^2 = 0.4$ line. So, in the regions of instability, the time rate of growth of the unstable waves decreases as the boundaries are approached.

In general, such inferences about the time-domain characteristics of the wave motion can be made from the stability charts, as these features are more or less valid also in other regions of the stability charts.

It should be noted that Figs. 8–10 are solutions of Eq. (11) and, therefore, they strictly show the time dependency of the wave pressures for an observer moving with the mean flow. Having determined the time dependency of the wave pressures, the time dependency of the particle velocity follows from Eq. (21).

3.5. *Frequency characterization of the stability charts*

So far in the analysis, no reference has been made to the frequency of the wave motion. Strictly speaking, as will be apparent in Section 4, the frequency characterization is useful for the stable waves. However, since the $\beta^2 = 0$ axis of a stability chart is stable for all stability numbers, η, it can be used to convert the stability number scale to a frequency scale. The purpose of this section is to derive this scale transformation.

For an observer moving with the mean flow, since λ is purely imaginary for stable waves, the pressure perturbations will appear as amplitude modulated waves of 'carrier' frequency $\varpi = \mathrm{i}\lambda$. Then, it follows from Eq. (22) that $a_1 = -2\cos \varpi T$. Upon solving this equation with Eq. (35), or

Eq. (48), for $\beta^2 = 0$, the required scale transformation is found to be

$$\eta = \frac{\varpi}{\Omega/2}. \tag{49}$$

Thus, the stability number is equal to the ratio of the frequency of the wave motion in the moving frame to half of the frequency of the ambient temperature variations. The regions of stability occur away from some vicinity of the frequencies $\varpi = n\Omega/2,\ n = 1, 2, 3, \ldots$.

It is more significant, however, to transform the stability number scale to the 'carrier' frequency that will be observed in a fixed frame. To obtain this transformation, first write Eq. (16) in the fixed co-ordinates:

$$p^{\mp}(\mathbf{x}, t) = B^{\mp}\Psi(x_2, x_3)\exp(\mp \mathrm{i}\sqrt{K^2 - \alpha^2}x_1)\varphi(t)\exp(\lambda \pm \mathrm{i}\sqrt{K^2 - \alpha^2}v_{o1})t, \tag{50}$$

Next, introduce a real positive variable, ω, by the 'dispersion equation'

$$(\lambda + \mathrm{i}\omega)^2 + (K^2 - \alpha^2)v_{o1}^2 = 0. \tag{51}$$

Then, Eq. (50) becomes

$$p^{\mp}(\mathbf{x}, t) = B^{\mp}\Psi(x_2, x_3)\exp(\mp \mathrm{i}\sqrt{K^2 - \alpha^2}x_1)\varphi(t)\exp(-\mathrm{i}\omega t). \tag{52}$$

Thus, to a fixed observer, the pressure perturbations will appear as amplitude modulated waves with 'carrier' frequency ω. Since the characteristic exponents are purely imaginary for stable waves, Eq. (51) can be expressed as

$$a_1 = -2\cos(\omega T \pm T\sqrt{K^2 - \alpha^2}v_{o1}). \tag{53}$$

Upon solving this equation with Eq. (35), or Eq. (48), for $\beta^2 = 0$, the required scale transformation between the stability number and the wave frequency in the fixed frame is obtained as

$$\frac{\omega}{\Omega/2} = \eta \mp \sqrt{\eta^2 - \left(\frac{\alpha\bar{c}_o}{\Omega/2}\right)^2}\bar{M}. \tag{54}$$

Here, $\bar{M} = v_{o1}/\bar{c}_o$ denotes the Mach number of the mean flow velocity based on the time averaged speed of sound. Eq. (54) shows that different scale transformations are required for each single-mode component. Note that, for $\eta < 2\alpha\bar{c}_o/\Omega$ (or, $K < \alpha$), ω becomes complex and the frequency characterization is not possible. If the mean flow is zero, Eq. (54) reduces to

$$\eta = \frac{\omega}{\Omega/2}, \tag{55}$$

as can be expected in view of Eq. (49). On the other hand, for plane waves (i.e., $\alpha = 0$), it becomes

$$\eta = \frac{1}{1 \mp \bar{M}}\frac{\omega}{\Omega/2}. \tag{56}$$

In general, the inverse of the scale transformation (54) can be expressed as the first of the equations

$$\eta = \frac{1 \pm \bar{M}A}{1 - \bar{M}^2}\frac{\omega}{\Omega/2}, \qquad A = \sqrt{1 - \frac{\alpha^2}{\bar{k}^2}(1 - \bar{M}^2)}, \qquad \bar{k} = \frac{\omega}{\bar{c}_o}. \tag{57}$$

As K^2 (and, therefore, η) is restricted to real positive values, it is clear from the second of the foregoing equations that the present stability charts apply only for the frequencies $\omega > \alpha\bar{c}_o\sqrt{1-\bar{M}^2}$.

It transpires from this analysis that the regions of stability occur away from some vicinity of the frequencies $\omega = n\Omega/2,\ n = 1, 2, 3, \ldots$, the frequencies corresponding to the boundaries of stability being dependent on the time-averaged mean flow Mach number $\bar{M}$ and the transverse eigenvalue α.

4. Transmission of the stable waves

4.1. Forward and backward propagating waves

The purpose of this section is to show the main features of stable wave propagation in a duct with time-variant ambient temperatures. The starting point of the analysis is Eq. (57), which is valid for the stable waves. Upon using this equation, Eq. (50) can be recast as

$$p^{\mp}(\mathbf{x}, t) = B^{\mp}\Psi(x_2, x_3)\exp(\mathrm{i}\bar{k}K_1^{\mp}x_1)\varphi(t)\exp(-\mathrm{i}\omega t). \tag{58}$$

Here

$$K_1^{\mp} = -\frac{\bar{M} \pm A}{1-\bar{M}^2}, \tag{59}$$

which are the familiar axial propagation constants of a uniform duct with $\exp(-\mathrm{i}\omega t)$ time dependence, constant speed of sound $\bar{c}_o$ and mean flow of Mach number $\bar{M}$ [1]. Eq. (57) shows that A is complex below the frequency $\omega = \bar{c}_o\alpha\sqrt{1-\bar{M}^2}$, which is the so-called cut-off frequency of a uniform duct with a constant speed of sound. The cut-off duct modes, which are said to be evanescent, are out of the scope of the present analysis, as K^2 is restricted to real positive values. For real values of A (i.e., propagating stable waves) it is convenient to associate the single-mode sound pressure components $p^+(\mathbf{x}, t)$ and $p^-(\mathbf{x}, t)$, which correspond to the propagation constants K^+ and K^-, respectively, with waves propagating in $+x_1$ (forward) and $-x_1$ (backward) directions, although the $+$ and $-$ signs of A may not necessarily correspond to positive and negative phase velocities in x_1 direction.

The velocity potential corresponding to the single-mode components of the stable waves are found from Eq. (19) and can be expressed similarly in the fixed co-ordinates:

$$\phi^{\mp}(\mathbf{x}, t) = \frac{B^{\mp}\bar{c}_o^2}{\mathrm{i}\omega p_o\gamma}\Psi(x_2, x_3)\left[\frac{1-\bar{M}^2}{1\pm\bar{M}A}\right]\exp(\mathrm{i}\bar{k}K_1^{\mp}x_1)\Phi(t)\exp(-\mathrm{i}\omega t), \tag{60}$$

where

$$\Phi(t) = \varphi(t) - \frac{1}{\mathrm{i}\omega}\frac{1-\bar{M}^2}{1\pm\bar{M}A}\frac{\mathrm{d}\varphi}{\mathrm{d}t}. \tag{61}$$

The components of the particle velocity corresponding to the forward and backward wave systems then follows from $\mathbf{v}^{\mp}(\mathbf{x}, t) = \nabla\phi^{\mp}(\mathbf{x}, t)$. In particular, the axial component of the particle

velocity is given by

$$v_1^{\mp}(\mathbf{x},t) = -\frac{B^{\mp}\bar{c}_o}{p_o\gamma}\Psi(x_2,x_3)\left[\frac{\bar{M}\pm A}{1\pm\bar{M}A}\right]\exp(\mathrm{i}\bar{k}K_1^{\mp}x_1)\Phi(t)\exp(-\mathrm{i}\omega t), \tag{62}$$

which can be expressed also as

$$v_1^{\mp}(\mathbf{x},t) = -\frac{\bar{c}_o}{p_o\gamma}\left[\frac{\bar{M}\pm A}{1\pm\bar{M}A}\right]\left[\frac{\Phi(t)}{\varphi(t)}\right]p^{\mp}(\mathbf{x},t). \tag{63}$$

Note that the axial velocity components have parts that are both in-phase and in-quadrature with the pressure wave components. The in-phase component is the same as that of the usual acoustic waveguide theory with a constant speed of sound (see, for example, Ref. [4]). The in-quadrature component is peculiar to the present theory.

It may be of interest to note that, if the sign of the time dependency is reversed, by putting $-\omega$ for ω in Eq. (51), this will result in the reversal of the signs of both exponents in Eqs. (58) and (60), as can be expected.

4.2. Axial admittance of the stable waves

The modulating function $\varphi(t)$ is periodic of period T and can be expanded into a Fourier series

$$\varphi(t) = \sum_{n=-\infty}^{\infty} F_n \exp(\mathrm{i}n\Omega t), \tag{64}$$

where F_n denote the complex Fourier coefficients. Hence, Eqs. (58) and (62) can be expressed, respectively, as

$$p^{\mp}(\mathbf{x},t) = P^{\mp}(\mathbf{x})\sum_{n=-\infty}^{\infty} F_n \exp[\mathrm{i}(n\Omega-\omega)t], \tag{65}$$

$$v_1^{\mp}(\mathbf{x},t) = P^{\mp}(\mathbf{x})\sum_{n=-\infty}^{\infty} F_n Y_n^{\mp}(\mathbf{x}) \exp[\mathrm{i}(n\Omega-\omega)t], \tag{66}$$

where

$$P^{\mp}(\mathbf{x}) = B^{\mp}\Psi(x_2,x_3)\exp(\mathrm{i}\bar{k}K_1^{\mp}x_1), \tag{67}$$

$$Y_n^{\mp} = -\frac{\bar{c}_o}{\gamma p_o}\left[\frac{\bar{M}\pm A}{1\pm\bar{M}A}\right]\left[1-\frac{n\Omega}{\omega}\left[\frac{1-\bar{M}^2}{1\pm\bar{M}A}\right]\right]. \tag{68}$$

Thus, the Fourier spectrum of a stable wave consists of the spectrum of the modulating function displaced on both sides of the frequency axis by ω. The wave motion will be periodic only if ω is an integer multiple of Ω, or, vice versa, it will be almost periodic. $Y_n^{\mp}$ is the axial modal admittance for the nth harmonic of the modulating function. The first term in Eq. (68) is the same as that of the classical acoustic waveguide theory with a constant speed of sound [4]. The second term, which is proportional to the harmonic number, is peculiar to the present theory.

4.3. Acoustic intensity of the stable waves

The determination of the acoustic intensity of stable waves in a duct with a time-varying ambient temperature is prone to some difficulties. In the classical acoustic waveguide theory, in which the speed of sound is assumed to be constant, Eqs. (4) and (5) can be cast as an acoustic energy conservation law, from which the definition of sound intensity, which is generally known as the Morfey equation [5] for irrotational uniform entropy flow, is extracted. With the speed of sound being time-variant, however, Eqs. (4) and (5) cannot be manipulated into a similar equation of acoustic energy conservation. Therefore, the present analysis adopts the definition of sound intensity as the total energy flux (kinetic energy flux plus compression strain energy flux) in the fluid due to acoustic motion of the particles [6]. Then, the acoustic intensity vector is given by

$$\mathbf{N} = [\rho \mathbf{v}]'_A [p/\rho + \mathbf{v}\cdot\mathbf{v}/2]'_A, \tag{69}$$

where the subscript 'A' indicates that the acoustic part of the fluctuations are to be taken. Then, for the evaluation of this expression, it is necessary to partition the fluctuations of the fluid density into an acoustic part due to the wave motion, and a non-acoustic part due to time-variance of the ambient temperature. Since the ambient temperature variation is presumed to occur at constant pressure p_o, the corresponding density variation is given by $\rho_o(t) = \gamma p_o/c_o^2(t)$. This can be decomposed into a Fourier series as $\rho_o(t) = \bar{\rho}_o + \rho'_o$, where the mean part is given by $\bar{\rho}_o = \gamma p_o/\bar{c}_o^2$, and the fluctuating part, ρ'_o, is assumed to be non-acoustic. Having separated the non-acoustic part, the expression for fluid density to be put in Eq. (69) may be taken as $\rho = \bar{\rho}_o + \rho'_A$. Upon assuming that this is related to the pressure fluctuations adiabatically (with the coefficients of specific heat at constant volume and pressure being assumed to be constant), the acoustic part of the density fluctuations, ρ'_A, can be computed by the well-known approximate relationship $\rho'_A = p'/c_o^2$. Hence, Eq. (69) is expressed, approximately, and to second order in the fluctuating quantities, as

$$\mathbf{N} = (\bar{\rho}_o \mathbf{v}' + p'\mathbf{v}_o/c_o^2)(p'/\bar{\rho}_o + \mathbf{v}_o\cdot\mathbf{v}). \tag{70}$$

The axial component of this vector, N_1, determines the sound power transmitted along the duct. In time-averaged form, this is given by

$$\bar{N}_1 = \overline{p'v'_1} + v_{o1}^2 \overline{p'v'_1/c_o^2} + \bar{\rho}_o v_{o1} \overline{(v'_1)^2} + v_{o1}\overline{(p'/c_o)^2}/\bar{\rho}_o, \tag{71}$$

where the overbar denotes time-averaging. Since $c_o(t)$ is always greater than zero and has the same period as $\varphi(t)$, it is expedient to introduce the following expansion for a formal computation of Eq. (71):

$$\varphi(t)/c_o(t) = \sum_{n=-\infty}^{\infty} C_n \exp(\mathrm{i}n\Omega t), \tag{72}$$

where C_n denotes complex Fourier coefficients. Hence, from Eqs. (65) and (66),

$$p^{\mp}(\mathbf{x},t)/c_o(t) = P^{\mp}(\mathbf{x}) \sum_{n=-\infty}^{\infty} C_n \exp[\mathrm{i}(n\Omega - \omega)t], \tag{73}$$

$$v_1^{\mp}(\mathbf{x},t)/c_o(t) = P^{\mp}(\mathbf{x}) \sum_{n=-\infty}^{\infty} C_n Y_n^{\mp} \exp[\mathrm{i}(n\Omega - \omega)t]. \tag{74}$$

The axial acoustic intensity for a single mode can be computed now by noting that, for a reflective field,

$$p'(\mathbf{x},t) = p^+(\mathbf{x},t) + p^-(\mathbf{x},t), \qquad v_1'(\mathbf{x},t) = v_1^+(\mathbf{x},t) + v_1^-(\mathbf{x},t). \tag{75}$$

Thus, upon using Eqs. (65), (66), (73) and (74), Eq. (71) can be expressed as

$$2\bar{N}_1 = A^+|P^+(\mathbf{x})|^2 + B[P^+(\mathbf{x})\breve{P}^-(\mathbf{x})]_R + A^-|P^-(\mathbf{x})|^2. \tag{76}$$

Here, the subscript 'R' denotes the real part of a complex quantity, the overarc denotes complex conjugate and the coefficients $A^{\pm}$ and B are given by

$$A^{\mp} = \sum_{n=-\infty}^{\infty} (1 + \bar{\rho}_o v_{o1} Y_n^{\mp})(Y_n^{\mp}|F_n|^2 + v_{o1}|C_n|^2/\bar{\rho}_o), \tag{77}$$

$$B = \sum_{n=-\infty}^{\infty} [(Y_n^+ + Y_n^- + 2\bar{\rho}_o v_{o1} Y_n^+ Y_n^-)|F_n|^2 + v_{o1}(2 + \bar{\rho}_o v_{o1}(Y_n^+ + Y_n^-)|C_n|^2)/\bar{\rho}_o)]. \tag{78}$$

In the case of zero mean flow, $v_{o1} = 0$,

$$Y_n^{\mp} = \frac{\mp \bar{c}_o A(1 - n\Omega/\omega)}{p_o \gamma}. \tag{79}$$

Therefore, $B = 0$ and Eq. (76) simplifies to

$$\bar{N}_1 = \frac{\bar{c}_o A}{2p_o\gamma}\left[\sum_{n=-\infty}^{\infty} (1 - n\Omega/\omega)|F_n|^2\right][|P^+(\mathbf{x})|^2 - |P^-(\mathbf{x})|^2]. \tag{80}$$

In the case of a constant speed of sound, $n = 0$, $F_0 = 1$, $C_0 = 1/\bar{c}_o$ and Eqs. (77) and (78) give $B = 0$ and

$$A^{\mp} = \frac{\mp A\bar{c}_o}{\gamma p_o}\left[\frac{1 - \bar{M}^2}{1 \pm \bar{M}A}\right]^2. \tag{81}$$

Therefore, for the constant speed of sound case, Eq. (76) reduces to the Morfey equation for axial intensity [4].

Implementation of Eq. (76), or (80), requires knowledge of the modulating function $\varphi(t)$. For the solutions given in Sections 3.2 and 3.3, $\varphi(t)$ can be determined by noting that, for the stable waves, the characteristic exponents are given by $\lambda = \pm \mathrm{i}\varpi$, and recasting the expressions for $q(t)$ to emulate Eq. (15). In general, however, given the solution of Eq. (11), the complex Fourier coefficients can be determined from the discrete Fourier transform of Eq. (15) or, from the T periodic solution of the differential equation for $\varphi(t)$, which can be derived by using Eq. (15) in Eq. (11). The summations in Eq. (76), or (80), need be taken only through the significant harmonics.

5. Some implications of the results for IC engine exhaust pipes

This section presents a discussion of some implications of the present theory for exhaust pipes. The theory has some relevance to engine exhaust noise, as the envisaged temperature condition is approximately satisfied in exhaust pipes. Of course, the approximation of the actual temporal variations of the temperature by a periodic function that is instantaneously uniform along some length of a pipe entails some simplification of reality; however, the essential effects of the temperature time-variance are captured by this simple model, providing further insight into the characteristics of engine exhaust noise.

In a standard IC engine, the dominant exhaust noise source is the blow-down pulse of hot gas mass. At every port, this mass injection occurs with a period equal to the reciprocal of the firing cycle frequency (FCF), which is equal to the number of crankshaft revolutions per second, N, say, for a two-stroke engine and to $N/2$ for a four-stroke engine. The sound waves generated by this process consist of all harmonics of the FCF and usually have a decaying spectrum.

Then, first considering a pipe that carries a single port flow, one has $T = 1/FCF$, since the blow-down temperature pulse and the exhaust gas mass injection may be assumed to occur with the same frequency. Hence, it can be concluded from the stability charts that, sound wave motion at frequencies that are in some vicinity of $\omega = 2\pi n \cdot (FCF/2)$, $n = 1, 2, 3, \ldots$; that is, all even harmonics, are likely to be unstable. Instability does not mean that wave motion should eventually blow up with an infinite amplitude; as amplitudes increase, non-linear effects get involved and hinder the development of larger amplitudes, resulting in finite amplitude waves.

In multi-cylinder engines, the situation is complicated by the fact that, as the hot exhaust gas flows downstream of a port, it merges with similar flows from the other ports. The actual temperature variations in merged flows are governed by complex heat transfer and fluid dynamic processes; however, for time intervals that are small compared to the thermal time constant associated with heat transfer, the temperature variations in a pipe that carries joining flows may be modelled approximately by juxtaposing, with appropriate phases, the temperature variations of the joining flows. Then, the above conclusion on the instability of the even harmonics applies also for pipes that carry joining flows, although the widths of the instability regions may be different due to the difference in temperature pulse shapes, certain harmonics may be more emphasized than the others due to interference, and instability at some odd harmonics may also be included, as will be shown presently. Here, it suffices to consider the exhaust pipe, the pipe where all port flows merge, as a representative case of a pipe that carries joining flows.

Assuming that the cylinders discharge at equal intervals and that the juxtaposed temperature variations for an exhaust pipe consist of identical elementary pulses that repeat at the same intervals, one has $T = 1/FFF$, where FFF abbreviates the 'fundamental firing frequency', which is equal to the number cylinders times the FCF. For this basic period, it can similarly be concluded that, all even harmonics of the FFF are likely to be unstable. The orders of these harmonics as multiples of the FCF depend on the number of cylinders. For an engine with an odd number of cylinders, all even harmonics of the FCF that are multiples of 4 are included in the unstable frequencies. For an engine with an even number of cylinders, on the other hand, all harmonics of the FCF are included if the number of cylinders is a multiple of 4, else, only the even harmonics are included.

The foregoing conclusions should be shaped for specific cases by inspection of the stability charts. The temporal variations of the exhaust gas temperature, and, hence, β^2, quickly decreases as the exhaust gas travels towards the tailpipe. Thus, an obvious implication of the stability charts is that, wave instabilities are more likely to originate closer to the engine, since the regions of instability gradually disappear as β^2 decreases and damping has stabilizing effect for small β^2. For a warmed up engine β^2 would be relatively small, but it can be quite large under exacting cold running conditions.

On the other hand, some regions of instability veer away from the $\omega = n\Omega/2$ frequencies as β^2 increases, thus stabilizing the harmonics corresponding to these frequencies. Also note that the presence of mean flow will push the stability boundaries to slightly higher (lower) frequencies for the forward (backward) propagating waves.

Figs. 3–5 indicate a tendency for the widths of the instability regions to increase with a, the duration of the temperature pulse as a fraction of the period T, although this is not uniform for all β^2 and the order of the instability region. For a pipe that carries a single port flow, the periodic rectangular function representation with $a \approx 0.25$ may be considered to be a reasonable approximation in a four-stroke cycle under steady running conditions. In the case of cold running conditions, the periodic right triangular function may be the slightly more realistic form of approximate representation with a value of a that is somewhat less than 0.25.

For an exhaust pipe of a multi-cylinder engine, the temperature variations may be modelled as periodic rectangular or right triangular pulses, the amplitudes, and hence β^2, being larger in the cold running engine case. Moreover, since the basic period of the temperature pulses is now $T = 1/FFF$, the value of the parameter a will be substantially larger than that for a pipe that carries a single-port flow. In general, joining flows tend to even out the temperature variations, however, for a cold engine, this effect is less significant and the reduction in β^2 may not be substantial. On these premises, it appears that the instabilities are more likely to be excited under cold running conditions and at the exhaust pipe, if they have not already been excited upstream.

The implications of the present theory support the proposition that the experimentally observed rasping noise may basically be a wave instability phenomena of the type considered in this paper. An account of the previous work on rasping noise, which is also called abnormal noise, has recently been given by Ayadi et al. [7], who have also presented an experimental study on the occurrence and signal analysis of the rasping noise. A 102 kW four cylinder gasoline engine with a real exhaust system without an auxiliary muffler was tested. Rasping noise occurred when the engine started and quickly accelerated under cold conditions. It is greatly reduced as the exhaust system warmed up. Order analysis showed high levels for orders up to the 100th, the high-frequency components having been developed along the intermediate pipe between the catalytic converter and the rear muffler. The authors have proposed that the generation of rasping noise may be caused by non-linear resonance phenomena, earlier authors having proposed the formation of shock waves as a possible cause of the rasping noise.

The experimentally observed conditions for the occurrence of the rasping noise are in fairly close agreement with the conditions of occurrence, and the conditions that enhance the likelihood of occurrence, of the wave instabilities predicted by the present theory. Although in Ref. [7] the authors tend to reject the proposition that rasping noise may be caused by formation of shock waves, the present theory does not exclude this possibility. Once instabilities are generated, wave

amplitudes will grow rapidly and non-linear phenomena will intervene, which may lead to non-linear resonance, or shock waves, in some parts of the system, if the conditions are favorable.

6. Conclusion

The classical theory of sound wave propagation in a homogeneous duct carrying a uniform mean flow has been extended by allowing for periodic temporal variations of the duct temperature. The present theory predicts unstable wave propagation in certain frequency bands. These instabilities have some relevance to engine exhaust noise. For unstable waves, the theory is not valid as amplitudes become large and non-linear effects get involved. A formal expression has been derived for the axial intensity of the stable waves.

Stability charts have been given for periodic rectangular and right-triangular pulse models of temperature variations. Stability charts for more realistic forms of temperature variations can also be derived similarly; however, this will, in general, require numerical integration. It is believed that, the solution of the Hill equation for the periodic right-triangular function is presented here for the first time. This solution can be used to construct stability charts for any function that can be approximated piecewise linearly.

References

[1] P.O.A.L. Davies, Waveguides, in: M.J. Crocker (Ed.), Encyclopedia of Acoustics, Vol. 1, Chapter 8, Wiley, New York, 1997.
[2] P.M. Morse, K.U. Ingard, Theoretical Acoustics, McGraw-Hill, New York, 1968.
[3] V.V. Bolotin, The Dynamic Stability of Elastic Systems, Holden-Day, San-Francisco, 1964.
[4] C.L. Morfey, Sound transmission and generation in ducts with flow, Journal of Sound and Vibration 14 (1) (1971) 37–55.
[5] C.L. Morfey, Acoustic energy in non-uniform flows, Journal of Sound and Vibration 14 (2) (1971) 159–170.
[6] E. Dokumaci, On calculation of acoustic power, Journal of Sound and Vibration 238 (5) (2000) 869–876.
[7] M. Ayadi, S. Frikha, P.-Y. Hennion, R. Willats, Characterization of rasping noise in automotive engine exhaust ducts, Journal of Sound and Vibration 244 (10) (2001) 79–106.